

The next-to-leading order QCD corrections to the production of B_c and B_c^* through the W^+ -boson decays

Xu-Chang Zheng^{a,*}, Chao-Hsi Chang^{b,c,d,†}, Xing-Gang Wu^{a,‡}, Jun Zeng^{a,§} and Xu-Dong Huang^{a,¶}

^a *Department of Physics, Chongqing University, Chongqing 401331, P.R. China.*

^b *Key Laboratory of Theoretical Physics, Institute of Theoretical Physics, Chinese Academy of Sciences, Beijing 100190, China.*

^c *School of Physical Sciences, University of Chinese Academy of Sciences, Beijing 100049, China.*

^d *CCAST (World Laboratory), Beijing 100190, China*

In this paper, we calculate the total decay widths for the W^+ -boson decays, $W^+ \rightarrow B_c + b + \bar{s} + X$ and $W^+ \rightarrow B_c^* + b + \bar{s} + X$, up to next-to-leading order (NLO) accuracy within the framework of the non-relativistic QCD theory. Both the fixed-order and the fragmentation approaches are adopted to do the calculation. Differential decay widths $d\Gamma/dz$ and $d\Gamma/ds_1$ are also given. We find that the NLO corrections are significant in those two W^+ decay channels. And our numerical results show that at the LHC, there are about 7.03×10^4 B_c meson events and 5.10×10^4 B_c^* meson events to be produced via the W^+ -boson decays per operation year.

PACS numbers: 12.38.Bx, 13.87.Fh, 13.66.Bc

I. INTRODUCTION

The $(c\bar{b})$ -quarkonium is a unique system in the Standard Model (SM) which carries two different heavy flavors. Studies on its production, decay and mass spectrum and etc. provide us a good platform to understand the strong and weak interactions deeply. The ground state B_c meson was first observed by the CDF collaboration at the Tevatron [1] and it attracts lots of interests since then. At present, the direct production of B_c meson and its excited states have been studied extensively in pp [2–18], e^+e^- [19–23] and ep [24, 25] collisions.

Besides the direct production mechanisms, the B_c meson can also be indirectly produced through the top-quark [26–28], the Z^0 -boson [29–33], the Higgs-boson [34, 35] and the W -boson [36–38] decays. These indirect production channels can also generate abundant B_c mesons at the LHC or the future high-energy colliders. The W -boson is the propagating media for the weak interaction, and the study on it is important for testing the SM. The LHC is a fruitful W -boson factory, there are about 3.07×10^{10} W -bosons to be produced at the LHC per operation year [36]. In the paper, we shall concentrate on the production of the B_c meson and its first excited state B_c^* meson through the W -boson decays.

The heavy constituent quarks move non-relativistically in the B_c meson, and the processes involving the B_c meson can be calculated within the nonrelativistic QCD (NRQCD) factorization formalism [39]. Generally, the production cross-section or the decay width can be factorized into the product of the short-distance coefficients and the long-distance matrix elements. The short-

distance coefficients describe the production or decay rate of the heavy quark-antiquark pair, which can be perturbatively calculated in powers of the strong coupling constant $\alpha_s(m_Q)$. The non-perturbative long-distance matrix elements describe the formation of the B_c meson from the heavy quark-antiquark pair, which can be calculated through potential models or lattice QCD.

The excited states of the B_c meson shall directly or indirectly decay to the ground state B_c meson via electromagnetic or strong interactions with $\sim 100\%$ probability, so these excited states are important sources of the B_c meson. Moreover, the production of the excited state is also interesting by itself. So, in addition to the B_c meson production, we shall also consider the production of the spin-triplet 3S_1 state B_c^* . The production of B_c and B_c^* mesons via the W -boson decays at the leading order (LO) level has been studied in Refs.[36, 37]. Since the masses of b and c quarks are not too large compared to the QCD asymptotic scale Λ_{QCD} , the higher-order QCD corrections could be important. In this paper, we shall study the $B_c^{(*)}$ meson production via the W -boson decays up to next-to-leading order (NLO) accuracy.

Any physical observable is independent of the renormalization scale, but there is renormalization scale ambiguity for the fixed-order pQCD predictions since one usually guesses the renormalization scale (e.g. usually setting as the one to eliminate large logs and etc.) and varies it over an arbitrary range to ascertain its uncertainty. This ambiguity introduces an important systematic error to pQCD predictions. It has been pointed out that one can use the higher-order β -terms to achieve an effective value of the strong running coupling α_s , and the resultant conformal series is independent to the choice of renormalization scale and thus the conventional renormalization ambiguity is eliminated [40–42]. The principle of maximum conformality (PMC) has been designed for such purpose [43–47], which provides a systemic way to eliminate the renormalization scheme-and-scale ambiguities simultaneously. The key idea of PMC is to set

* zhengxc@cqu.edu.cn

† zhangzx@itp.ac.cn

‡ wuxg@cqu.edu.cn

§ zengj@cqu.edu.cn

¶ hxud@cqu.edu.cn

the correct momentum flow of the process by absorbing the non-conformal β -terms that govern the behavior of α_s through the renormalization group equation (RGE). As a byproduct, due to the elimination of the divergent renormalon terms, the convergence of the pQCD series can be naturally improved. The β_0 -terms in the NLO coefficients can be adopted to set the α_s value, thus in the paper, in addition to the conventional treatment, we shall also adopt the PMC to deal with the W^+ -boson decays, $W^+ \rightarrow B_c^{(*)} + b + \bar{s} + X$.

In the decays, $W^+ \rightarrow B_c^{(*)} + b + \bar{s} + X$, the involved hard scales satisfy, $m_W \gg m_b, m_c$, so it is expected that the fragmentation mechanism dominates those decays. The NLO fragmentation functions for a heavy quark to a B_c or B_c^* have recently been given by Ref.[23]. It is interesting to apply those NLO fragmentation functions to the present processes, and compare the results from the fragmentation approach with those from the fixed-order approach. And in the present paper, besides the fixed-order approach, we shall also adopt the fragmentation approach to do the calculation. In usual cases, because the fragmentation probability of $\bar{b} \rightarrow B_c$ is about two orders of magnitude larger than that of $c \rightarrow B_c$, the \bar{b} fragmentation is generally more important than the c fragmentation for the B_c meson production. However, in cases with the W^+ -boson decays, the decay width for the \bar{b} fragmentation shall be depressed due to the small values of the CKM matrix elements $|V_{cb}|$ and $|V_{ub}|$; Thus, it provides a good platform to test the fragmentation function for $c \rightarrow B_c$.

The paper is organized as follows. In Sec.II, we briefly present useful formulas at the LO accuracy under the fixed-order approach. In Sec.III, we present the formulas to calculate the NLO QCD corrections for the $B_c^{(*)}$ meson production through the W -boson decays under the fixed-order approach. In Sec.IV, we present the useful formulas to calculate the decay widths under the fragmentation approach up to NLO accuracy. In Sec.V, numerical results and discussions are presented. Sec.VI is reserved as a summary.

II. DECAY WIDTHS AT THE LO LEVEL

According to the NRQCD factorization, the differential decay width for the B_c -meson production from the W^+ -boson decays can be written as

$$d\Gamma_{W^+ \rightarrow B_c + b + \bar{s} + X} = \sum_n d\tilde{\Gamma}_{W^+ \rightarrow (c\bar{b})[n] + b + \bar{s} + X} \langle \mathcal{O}^{B_c}(n) \rangle, \quad (1)$$

where $d\tilde{\Gamma}_{W^+ \rightarrow (c\bar{b})[n] + b + \bar{s} + X}$ denotes the decay width for the production of a perturbative state $(c\bar{b})[n]$ with quantum numbers $[n]$. The long-distance matrix element $\langle \mathcal{O}^{B_c}(n) \rangle$ is the transition probability for a $(c\bar{b})[n]$ state to the B_c meson. In the lowest-order nonrelativistic approximation, only color-singlet contributions need to be

considered, and the long-distance matrix elements for the color-singlet contributions can be determined through potential models.

Practically, we first calculate the decay width for an on-shell $(c\bar{b})$ -pair, i.e., $d\Gamma_{W^+ \rightarrow (c\bar{b})[n] + b + \bar{s} + X}$. Then the decay width for the B_c meson, i.e., $d\Gamma_{W^+ \rightarrow B_c + b + \bar{s} + X}$, can be obtained from $d\Gamma_{W^+ \rightarrow (c\bar{b})[n] + b + \bar{s} + X}$ by replacing $\langle \mathcal{O}^{(c\bar{b})[n]}(n) \rangle$ by $\langle \mathcal{O}^{B_c}(n) \rangle$.

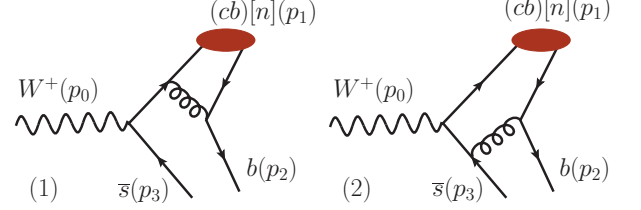


FIG. 1. The LO Feynman diagrams for $W^+ \rightarrow (c\bar{b})[n] + b + \bar{s}$.

At the LO level, there are two Feynman diagrams for the $(c\bar{b})[n]$ -pair production from the W^+ -boson decays, which are shown in Fig.1. The LO amplitude for the $(c\bar{b})[n]$ production can be written as the sum of two terms ($M_{LO} = M_1 + M_2$) corresponding to two Feynman diagrams in Fig.1, and we have

$$iM_1 = -\frac{igV_{cs}}{2\sqrt{2}} \frac{-i}{(p_{12} + p_2)^2 + i\epsilon} \bar{u}(p_2)(ig_s\gamma^\mu T^a) \cdot \Pi\Lambda_1(ig_s\gamma_\mu T^a) \frac{i}{\not{p}_1 + \not{p}_2 - m_c + i\epsilon} \cdot \epsilon_\nu(p_0)\gamma^\nu(1 - \gamma_5)v(p_3)|_{q=0}, \quad (2)$$

$$iM_2 = -\frac{igV_{cs}}{2\sqrt{2}} \frac{-i}{(p_{12} + p_2)^2 + i\epsilon} \bar{u}(p_2)(ig_s\gamma^\mu T^a)\Pi\Lambda_1 \cdot \epsilon_\nu(p_0)\gamma^\nu(1 - \gamma_5) \frac{i}{-\not{p}_0 + \not{p}_{11} - m_c + i\epsilon} \cdot (ig_s\gamma_\mu T^a)v(p_3)|_{q=0}, \quad (3)$$

where p_{11} and p_{12} are momenta of the c and \bar{b} quarks in $(c\bar{b})[n]$ -pair,

$$p_{11} = r_c p_1 - q, \quad p_{12} = (1 - r_c) p_1 + q, \quad (4)$$

where $r_c = m_c/(m_b + m_c)$. Π denotes the spin projector, for 1S_0 state,

$$\Pi = \frac{-\sqrt{M}}{4m_b m_c} (\not{p}_{12} - m_b)\gamma_5(\not{p}_{11} + m_c), \quad (5)$$

and for 3S_1 state,

$$\Pi = \frac{-\sqrt{M}}{4m_b m_c} (\not{p}_{12} - m_b)\not{\epsilon}(p_1)(\not{p}_{11} + m_c). \quad (6)$$

Λ_1 is color-singlet projector, and

$$\Lambda_1 = \frac{\mathbf{1}}{\sqrt{3}}, \quad (7)$$

where $\mathbf{1}$ denotes the unit matrix of the color $SU(3)$ group.

Using those amplitudes at the LO level, the LO decay width for $(c\bar{b})$ -pair production can be calculated through

$$d\Gamma_{\text{LO}}^{(c\bar{b})[n]} = \frac{1}{3} \frac{1}{2m_W} \sum |M_{\text{LO}}|^2 d\Phi_3, \quad (8)$$

where \sum denotes the sum over the color and spin states of the initial and final particles, $1/3$ comes from the spin average of the initial W^+ -boson. $d\Phi_3$ denotes the differential phase space at the LO level,

$$d\Phi_3 = (2\pi)^d \delta^d \left(p_0 - \sum_{f=1}^3 p_f \right) \prod_{f=1}^3 \frac{d^{d-1} \mathbf{p}_f}{(2\pi)^{d-1} 2E_f}, \quad (9)$$

where d stands for the dimension of the space-time. With these formulas, the LO decay width for $W^+ \rightarrow (c\bar{b})[n] + b + \bar{s} + X$ can be calculated directly.

III. THE NLO QCD CORRECTIONS

The NLO QCD corrections to the decay widths include virtual and real corrections. There are ultraviolet (UV) and infrared (IR) divergences in virtual correction, and IR divergence in real correction. We adopt the conventional dimensional regularization approach with $d = 4 - 2\epsilon$ to regulate these divergences. Then the UV and IR divergences appear as pole terms in $1/\epsilon$. We shall sketch the calculations for the virtual and real corrections in the following subsections.

A. The virtual correction

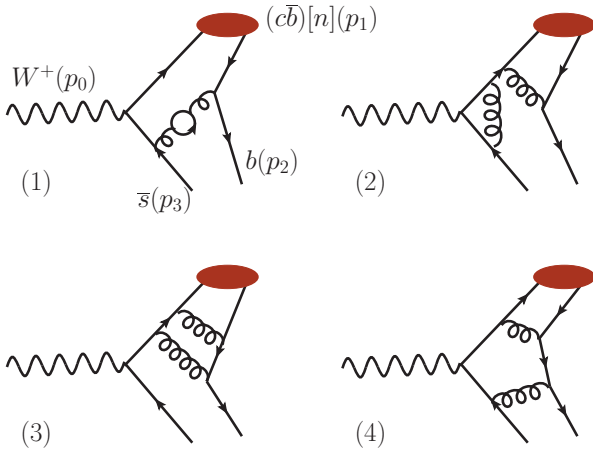


FIG. 2. Four typical one-loop Feynman diagrams for $W^+ \rightarrow c\bar{b}[n] + b + \bar{s}$.

Four typical one-loop diagrams are shown in Fig.2. The NLO virtual corrections come from the interference of those one-loop Feynman diagrams with the LO Feynman diagrams shown in Fig.1.

The virtual corrections can be calculated through

$$d\Gamma_{\text{Virtual}}^{(c\bar{b})[n]} = \frac{1}{3} \frac{1}{2m_W} \sum 2\text{Re}(M_{\text{LO}}^* M_{\text{Virtual}}) d\Phi_3, \quad (10)$$

where M_{Virtual} denotes the amplitude for the virtual corrections, $d\Phi_3$ is the LO differential phase space.

As a subtle point, there are Coulomb divergences in the hard part of the NLO amplitudes by using the traditional matching procedure. One may observe that they appear in both the virtual corrections to the $(c\bar{b})[n]$ production and the virtual corrections to the long-distance matrix element $\langle \mathcal{O}^{(c\bar{b})[n]}(n) \rangle$, which shall be canceled by each other. As a result, no Coulomb divergence appears in the resultant pQCD series. In dimensional regularization, there is a simpler way to extract the NRQCD short-distance coefficients using the method of regions [48]. In this method, one can calculate the hard region contributions directly by expanding the relative momentum of the $(c\bar{b})[n]$ pair before carrying out the loop integration (More explicitly, under the present lowest-order nonrelativistic approximation, one just needs to set $q = 0$ before the loop integration). We adopt this new treatment, and the Coulomb divergences, which come from the potential region, shall not appear in our present calculation.

There are UV and IR divergences in the loop-diagram contributions. The IR divergences in the virtual correction shall be canceled by the IR divergences in the real correction. The UV divergences should be removed through renormalization. We carry out the renormalization using counterterm approach, where the decay widths are calculated in terms of the renormalized quark mass m , the renormalized quark field Ψ_r , the renormalized gluon field A_r^μ , and the renormalized coupling constant g_s . The relations between the renormalized quantities and their corresponding bare quantities are

$$\begin{aligned} m_0 &= Z_m m, \quad \Psi_0 = \sqrt{Z_2} \Psi_r, \\ A_0^\mu &= \sqrt{Z_3} A_r^\mu, \quad g_s^0 = Z_g g_s, \end{aligned} \quad (11)$$

where $Z_i = 1 + \delta Z_i$ with $i = m, 2, 3, g$ are renormalization constants, and they are fixed by the renormalization scheme. The renormalization scheme is adopted as follows: The renormalization of the heavy quark mass, the heavy quark field and the gluon field are performed in the on-shell scheme, whereas the renormalization of the strong coupling constant is performed in the $\overline{\text{MS}}$ scheme. The quantities δZ_i can be calculated and they are

$$\begin{aligned} \delta Z_{m,Q}^{\text{OS}} &= -3 C_F \frac{\alpha_s}{4\pi} \left[\frac{1}{\epsilon_{UV}} - \gamma_E + \ln \frac{4\pi\mu_R^2}{m_Q^2} + \frac{4}{3} \right], \\ \delta Z_{2,Q}^{\text{OS}} &= -C_F \frac{\alpha_s}{4\pi} \left[\frac{1}{\epsilon_{UV}} + \frac{2}{\epsilon_{IR}} - 3\gamma_E + 3 \ln \frac{4\pi\mu_R^2}{m_Q^2} + 4 \right], \\ \delta Z_{2,q}^{\text{OS}} &= -C_F \frac{\alpha_s}{4\pi} \left[\frac{1}{\epsilon_{UV}} - \frac{1}{\epsilon_{IR}} \right], \end{aligned}$$

$$\delta Z_3^{OS} = \frac{\alpha_s}{4\pi} \left[(\beta'_0 - 2C_A) \left(\frac{1}{\epsilon_{UV}} - \frac{1}{\epsilon_{IR}} \right) - \frac{4}{3} T_F \left(\frac{1}{\epsilon_{UV}} - \gamma_E + \ln \frac{4\pi\mu_R^2}{m_c^2} \right) - \frac{4}{3} T_F \left(\frac{1}{\epsilon_{UV}} - \gamma_E + \ln \frac{4\pi\mu_R^2}{m_b^2} \right) \right],$$

$$\delta Z_g^{\overline{\text{MS}}} = -\frac{\beta_0}{2} \frac{\alpha_s}{4\pi} \left[\frac{1}{\epsilon_{UV}} - \gamma_E + \ln(4\pi) \right],$$

where $Q(=c, b)$ in the subscripts denotes a heavy quark, and $q(=s)$ denotes a light quark. μ_R is the renormalization scale, γ_E is the Euler constant. For QCD, $C_A = 3$, $C_F = 4/3$ and $T_F = 1/2$. $\beta_0 = 11C_A/3 - 4T_F n_f/3$ is the one-loop coefficient of the QCD β function, in which n_f is the number of active quark flavors. $\beta'_0 = 11C_A/3 - 4T_F n_{lf}/3$ and $n_{lf} = 3$ is the number light-quark flavors.

B. The real correction

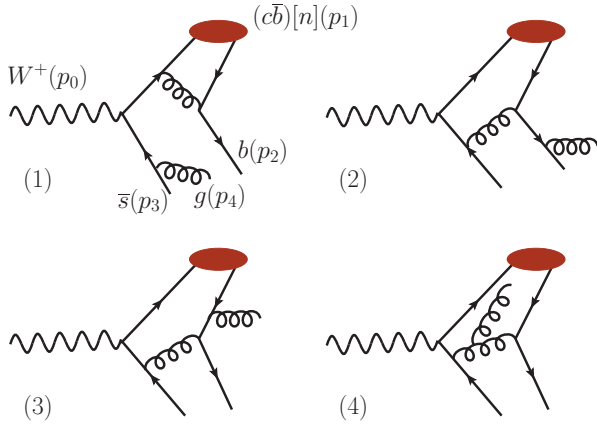


FIG. 3. Four typical real-correction Feynman diagrams for $W^+ \rightarrow (c\bar{b})[n] + b + \bar{s}$.

The real corrections come from the decay process $W^+(p_0) \rightarrow (c\bar{b})[n](p_1) + b(p_2) + \bar{s}(p_3) + g(p_4)$. The Feynman diagrams for the real corrections can be obtained through the LO Feynman diagrams by adding an additional gluon in the final state. Typical real correction Feynman diagrams are shown in Fig.3. The real correction can be calculated through

$$d\Gamma_{\text{Real}}^{(c\bar{b})[n]} = \frac{1}{3} \frac{1}{2m_W} \sum |M_{\text{Real}}|^2 d\Phi_4, \quad (12)$$

where $d\Phi_4$ denotes the differential phase space for the real corrections, and

$$d\Phi_4 = (2\pi)^d \delta^d \left(p_0 - \sum_{f=1}^4 p_f \right) \prod_{f=1}^4 \frac{d^{d-1} \mathbf{p}_f}{(2\pi)^{d-1} 2E_f}. \quad (13)$$

There are IR divergences in the real correction, which come from the phase-space integration. However, integrating the squared amplitude directly over the phase space in d dimensions is too difficult to be practical. In order to isolate the divergent and finite terms, we adopt the two-cutoff phase-space slicing method [49] to calculate the real correction. Following this method, the phase space for the real correction is decomposed into three regions by introducing two small cutoffs, δ_s and δ_c , which should satisfy the requirement $\delta_c \ll \delta_s$ [49]. The three regions are soft region (S) with $E_4 \leq m_W \delta_s/2$, hard-collinear region (HC) with $E_4 > m_W \delta_s/2$ and $(p_3 + p_4)^2 \leq \delta_c m_W^2$, and hard-non-collinear region (HNC) with $E_4 > m_W \delta_s/2$ and $(p_3 + p_4)^2 > \delta_c m_W^2$, where E_4 is defined in the rest frame of the initial W^+ boson. The IR finite hard-non-collinear part can be calculated numerically in four dimensions.

Applying the soft approximation to the soft part (e.g. all the terms of order δ_s are neglected), we obtain

$$d\Gamma_S^{(c\bar{b})[n]} = d\Gamma_{\text{LO}}^{(c\bar{b})[n]} \left[\frac{C_F \alpha_s}{2\pi} \frac{\Gamma(1-\epsilon)}{\Gamma(1-2\epsilon)} \left(\frac{4\pi\mu_R^2}{m_W^2} \right)^\epsilon \right] \cdot \left\{ \frac{1}{\epsilon^2} + \frac{1}{\epsilon} \left[1 - 2\ln\delta_s - \ln \left(\frac{(1-\beta_b \cos\theta)^2}{1-\beta_b^2} \right) \right] - 2\ln\delta_s + 2\ln^2\delta_s + 2\ln\delta_s \ln \left(\frac{(1-\beta_b \cos\theta)^2}{1-\beta_b^2} \right) + \frac{1}{\beta_b} \ln \left(\frac{1+\beta_b}{1-\beta_b} \right) + \ln^2 \left(\frac{1-\beta_b}{1-\beta_b \cos\theta} \right) - \frac{1}{2} \ln^2 \left(\frac{1+\beta_b}{1-\beta_b} \right) + 2\text{Li}_2 \left(-\frac{\beta_b(1-\cos\theta)}{1-\beta_b} \right) - 2\text{Li}_2 \left(-\frac{\beta_b(1+\cos\theta)}{1-\beta_b \cos\theta} \right) \right\}, \quad (14)$$

where $\beta_b = \sqrt{1-m_b^2/E_2^2}$, and E_2 is defined in the rest frame of the W^+ boson. θ is the angle between \mathbf{p}_2 and \mathbf{p}_3 in the rest frame of the W^+ boson.

Applying the collinear approximation (e.g. terms of order δ_c are neglected), we obtain

$$d\Gamma_{\text{HC}}^{(c\bar{b})[n]} = d\Gamma_{\text{LO}}^{(c\bar{b})[n]} \left[\frac{C_F \alpha_s}{2\pi} \frac{\Gamma(1-\epsilon)}{\Gamma(1-2\epsilon)} \left(\frac{4\pi\mu_R^2}{m_W^2} \right)^\epsilon \right] \times \left(\frac{A_1^{q \rightarrow qg}}{\epsilon} + A_0^{q \rightarrow qg} \right), \quad (15)$$

where

$$A_1^{q \rightarrow qg} = 3/2 + 2\ln\delta'_s, \quad (16)$$

$$A_0^{q \rightarrow qg} = 7/2 - \pi^2/3 - \ln^2\delta'_s - \ln\delta_c(3/2 + 2\ln\delta'_s), \quad (17)$$

and $\delta'_s = m_W^2 \delta_s / [m_W^2 - (p_1 + p_2)^2]$.

Summing up three parts from the soft, hard-collinear and hard-non-collinear regions, we obtain the required real correction. Separate contributions from three regions depend on one or both of the two cutoff parameters δ_s and δ_c . However, the sum of those three contributions should be independent to the choices of δ_s and δ_c . The

verification of this cut-off independence provides an important check for the correctness of the numerical calculation. We have checked this independence and have indeed found that the results are independent of the δ_s and δ_c by varying δ_s from 10^{-3} to 10^{-7} with $\delta_c = \delta_s/50$. For clarity, we fix $\delta_s = 10^{-5}$ and $\delta_c = 2 \times 10^{-7}$ to do the following numerical calculation.

Total NLO corrections can be obtained by summing up virtual and real corrections. The UV and IR divergences are exactly canceled after summing the real and virtual corrections, and the finite NLO corrections are obtained. Then the decay widths $\Gamma_{W^+ \rightarrow B_c + b + \bar{s} + X}$ and $\Gamma_{W^+ \rightarrow B_c^* + b + \bar{s} + X}$ can be derived from $\Gamma_{W^+ \rightarrow (c\bar{b})[{}^1S_0] + b + \bar{s} + X}$ and $\Gamma_{W^+ \rightarrow (c\bar{b})[{}^3S_1] + b + \bar{s} + X}$ by multiplying a factor $\langle \mathcal{O}^{B_c(B_c^*)}(n) \rangle / \langle \mathcal{O}^{(c\bar{b})[n]}(n) \rangle \approx |R_S(0)|^2/4\pi$, where $n = {}^1S_0$ for B_c and $n = {}^3S_1$ for B_c^* , respectively. $R_S(0)$ denotes the radial wave function at the origin of the $B_c(B_c^*)$ meson.

In the calculation, we adopt the FeynArts package [50] to generate the Feynman diagrams and the corresponding amplitudes, and the FeynCalc package [51, 52] to carry out the Dirac and color traces. Then we use the \$Apart package [53] and the FIRE package [54] to do partial fraction and integration-by-parts (IBP) reduction of the loop integrals. After the IBP reduction, there are only few master integrals (e.g. A_0 , B_0 , C_0 , and D_0 functions) need to be calculated, which shall be dealt with by using the LoopTools package [55]. Numerical phase-space integrations are carried out by the VEGAS program [56].

IV. DECAY WIDTHS UNDER THE FRAGMENTATION APPROACH

We take the process $W^+ \rightarrow B_c + X$ as an example to illustrate the calculation under the fragmentation approach. The formulas for the B_c^* production are similar to the B_c case.

The differential decay width for $W^+ \rightarrow B_c + X$ under the fragmentation approach can be written as

$$\frac{d\Gamma_{W^+ \rightarrow B_c + X}}{dz} = \sum_i \int_z^1 \frac{dy}{y} \frac{d\hat{\Gamma}_{W^+ \rightarrow i + X}(y, \mu_F)}{dy} D_{i \rightarrow B_c}(z/y, \mu_F), \quad (18)$$

where $d\hat{\Gamma}_{W^+ \rightarrow i + X}(y, \mu_F)$ denotes the decay width (coefficient function) for a W^+ to a parton i ¹, $D_{i \rightarrow B_c}(z/y, \mu_F)$ denotes the fragmentation function for a parton i into a

B_c , and μ_F is the factorization scale which separates the energy scales of two parts.

For comparison, we adopt several strategies to obtain the fragmentation predictions. More details about those strategies can be found in Refs.[23, 57]. For convenience, we denote them as “Frag, LO”, “Frag, NLO” and “Frag, NLO+NLL”, respectively. For the case of “Frag, LO”,

$$\begin{aligned} \frac{d\Gamma_{W^+ \rightarrow B_c + X}^{\text{Frag, LO}}}{dz} &= \int_z^1 \frac{dy}{y} \frac{d\hat{\Gamma}_{W^+ \rightarrow c + \bar{s}}^{\text{LO}}(y, \mu_F)}{dy} \\ &\quad \cdot D_{c \rightarrow B_c}^{\text{LO}}(z/y, \mu_F) \\ &= \Gamma_{W^+ \rightarrow c + \bar{s}}^{\text{LO}} \cdot D_{c \rightarrow B_c}^{\text{LO}}(z, \mu_F), \end{aligned} \quad (19)$$

where $\Gamma_{W^+ \rightarrow c + \bar{s}}^{\text{LO}}$ is the LO decay width for $W^+ \rightarrow c + \bar{s}$ and $D_{c \rightarrow B_c}^{\text{LO}}(z, \mu_F)$ is the LO fragmentation function. In the calculation, the factorization and renormalization scales are set as $\mu_F = 2m_b + m_c$ and $\mu_R = 2m_b$.

For the case of “Frag, NLO”,

$$\begin{aligned} \frac{d\Gamma_{W^+ \rightarrow B_c + X}^{\text{Frag, NLO}}}{dz} &= \int_z^1 \frac{dy}{y} \frac{d\hat{\Gamma}_{W^+ \rightarrow c + X}^{\text{NLO}}(y, \mu_F)}{dy} \\ &\quad \cdot D_{c \rightarrow B_c}^{\text{NLO}}(z/y, \mu_F), \end{aligned} \quad (20)$$

where the NLO fragmentation function $D_{c \rightarrow B_c}^{\text{NLO}}(z, \mu_F)$ can be found in Ref.[23]. In the calculation, the factorization and renormalization scales are set as $\mu_F = 2m_b + m_c$ and $\mu_R = 2m_b$, and the factorization scheme is chosen as the $\overline{\text{MS}}$ scheme.

For the case of “Frag, NLO+NLL”,

$$\begin{aligned} \frac{d\Gamma_{W^+ \rightarrow B_c + X}^{\text{Frag, NLO+NLL}}}{dz} &= \int_z^1 \frac{dy}{y} \frac{d\hat{\Gamma}_{W^+ \rightarrow c + X}^{\text{NLO}}(y, \mu_F)}{dy} \\ &\quad \cdot D_{c \rightarrow B_c}^{\text{NLO+NLL}}(z/y, \mu_F), \end{aligned} \quad (21)$$

where the factorization and renormalization scales in the coefficient function $d\hat{\Gamma}_{W^+ \rightarrow c + X}^{\text{NLO}}(y, \mu_F)/dy$ are set as $\mu_F = \mu_R = m_w$, so as to avoid the large logarithms of μ_F^2/m_w^2 or μ_R^2/m_w^2 appear in the coefficient function. The fragmentation function $D_{c \rightarrow B_c}^{\text{NLO+NLL}}(z, \mu_F = m_w)$ is obtained through solving the Dokshitzer-Gribov-Lipatov-Altarelli-Parisi (DGLAP) evolution equation [58–60] with NLO splitting function for $c \rightarrow c$ [61–63], where the NLO fragmentation function $D_{c \rightarrow B_c}^{\text{NLO}}(z, \mu_F = 2m_b + m_c)$ with $\mu_R = 2m_b$ is used as the boundary condition.

V. NUMERICAL RESULTS AND DISCUSSIONS

To do the numerical calculation, the input parameters are taken as follows:

$$\begin{aligned} m_b &= 4.9 \text{ GeV}, \quad m_c = 1.5 \text{ GeV}, \quad m_w = 80.4 \text{ GeV}, \\ G_F &= 1.166 \times 10^{-5} \text{ GeV}^{-2}, \quad |V_{cs}| = 1, \\ |R_S(0)|^2 &= 1.642 \text{ GeV}^3, \end{aligned} \quad (22)$$

¹ Due to the coefficient function $d\hat{\Gamma}_{W^+ \rightarrow i + X}(y, \mu_F)$ is IR safe, the heavy-quark mass m_Q in the coefficient function can be approximately set to 0, and this approximation brings only a small error of $\mathcal{O}(m_Q^2/m_w^2)$. In the following fragmentation calculations, we shall adopt this approximation for simplicity. The neglected higher-power terms will be included in the results by combining the fixed-order and fragmentation approaches.

where G_F is the Fermi coupling constant. The input value for $|R_S(0)|^2$ is taken from the potential-model calculation [64]. For the strong coupling constant, we use the two-loop formula

$$\alpha_s(\mu_R) = \frac{4\pi}{\beta_0 \ln(\mu_R^2/\Lambda_{QCD}^2)} \left[1 - \frac{\beta_1 \ln \ln(\mu_R^2/\Lambda_{QCD}^2)}{\beta_0^2 \ln(\mu_R^2/\Lambda_{QCD}^2)} \right],$$

where $\beta_1 = 34 C_A^2/3 - 4 T_F C_F n_f - 20 T_F C_A n_f/3$ is the two-loop coefficient of the QCD β -function. According to $\alpha_s(m_Z) = 0.1185$ [65], we obtain $\Lambda_{QCD}^{n_f=5} = 0.233$ GeV and $\Lambda_{QCD}^{n_f=4} = 0.337$ GeV.

A. Basic results

	$\Gamma_{LO}(\text{keV})$	$\Gamma_{NLO}^{\text{Cor.}}(\text{keV})$	$\Gamma_{NLO}(\text{keV})$	$\Gamma_{NLO}^{\text{Cor.}}/\Gamma_{LO}$
$\mu_R = 2m_b$	2.89	2.00	4.89	0.69
$\mu_R = m_W$	1.30	1.42	2.72	1.09

TABLE I. The total decay widths of $W^+ \rightarrow B_c + b + \bar{s} + X$ up to NLO level under the fixed-order approach. Two typical renormalization scales are adopted.

	$\Gamma_{LO}(\text{keV})$	$\Gamma_{NLO}^{\text{Cor.}}(\text{keV})$	$\Gamma_{NLO}(\text{keV})$	$\Gamma_{NLO}^{\text{Cor.}}/\Gamma_{LO}$
$\mu_R = 2m_b$	2.48	1.07	3.55	0.43
$\mu_R = m_W$	1.12	1.03	2.15	0.92

TABLE II. The total decay widths of $W^+ \rightarrow B_c^* + b + \bar{s} + X$ up to NLO level under the fixed-order approach. Two typical renormalization scales are adopted.

The decay widths for $W^+ \rightarrow B_c + b + \bar{s} + X$ and $W^+ \rightarrow B_c^* + b + \bar{s} + X$ under the fixed-order approach are given in Tables I and II, where $\Gamma_{NLO} = \Gamma_{LO} + \Gamma_{NLO}^{\text{Cor.}}$ and $\Gamma_{NLO}^{\text{Cor.}}$ denotes the NLO corrections, $\Gamma_{NLO}^{\text{Cor.}} = \Gamma_{\text{virtual}} + \Gamma_{\text{Real}}$. In the calculation, we take two typical energy scales ($2m_b$ and m_W) as the renormalization scale, and we have $\alpha_s(2m_b) = 0.180$ and $\alpha_s(m_W) = 0.121$. Tables I and II show that the NLO corrections are significant. After including the NLO corrections, the total decay width for $W^+ \rightarrow B_c(B_c^*) + b + \bar{s} + X$ is increased by 69% (43%) for $\mu_R = 2m_b$ and 109% (92%) for $\mu_R = m_W$.

The momentum of the produced b -quark jet can be measured using vertex tagging technology, so the invariant mass of the $B_c(B_c^*)$ and b quark in the final state can be determined experimentally. We present the differential decay widths $d\Gamma/ds_1$ for $W^+ \rightarrow B_c(B_c^*) + b + \bar{s} + X$ in Figs. 4 and 5, where $\mu_R = 2m_b$ and $\mu_R = m_W$, respectively. Here $s_1 \equiv (p_1 + p_2)^2$. Figs. 4 and 5 show that there is a peak near the minimum value of s_1 , indicating the dominant contributions of the decay processes come from the phase-space region near the threshold of producing the $B_c(B_c^*)$ and b quark. This property may be helpful to distinguish the B_c or B_c^* mesons produced

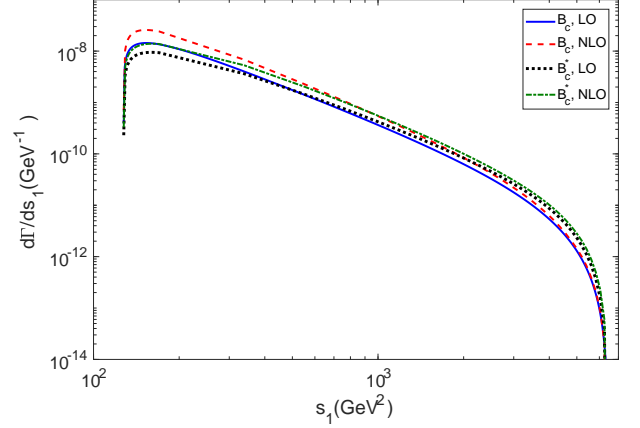


FIG. 4. Differential decay widths $d\Gamma/ds_1$ for $W^+ \rightarrow B_c(B_c^*) + b + \bar{s} + X$ under the fixed-order approach. $\mu_R = 2m_b$.

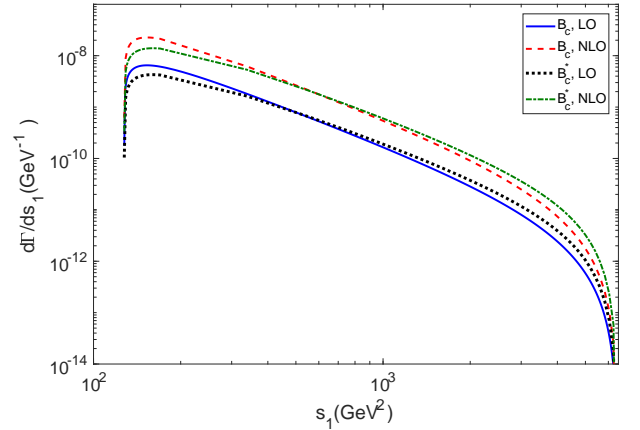


FIG. 5. Differential decay widths $d\Gamma/ds_1$ for $W^+ \rightarrow B_c(B_c^*) + b + \bar{s} + X$ under the fixed-order approach. $\mu_R = m_W$.

through the W^+ -boson decays from the those produced through other production mechanisms at the high-energy colliders.

Tables I and II show that after including the NLO corrections, the renormalization scale dependence is softened. However, such scale dependence is still very large, e.g. $W^+ \rightarrow B_c(B_c^*) + b + \bar{s} + X$, the NLO total decay width decreases by 44% (39%), when μ_R changes from $2m_b$ to m_W .

As mentioned in the Introduction, the PMC scale-setting approach provides a way to eliminate the renormalization scale ambiguity [43–47]. As an attempt of showing how the PMC affects the decay width, we present the PMC predictions in the following.

To apply the PMC, we first schematically rewritten the

NLO decay width as

$$\begin{aligned}\Gamma &= A \alpha_s^2(\mu_R) \left[1 + (a + b n_f) \frac{\alpha_s(\mu_R)}{\pi} \right] \\ &= A \alpha_s^2(\mu_R) \left\{ 1 + \left[-\frac{3b}{2} \beta_0 + \left(a + \frac{33b}{2} \right) \right] \frac{\alpha_s(\mu_R)}{\pi} \right\} \quad (23)\end{aligned}$$

Using the RGE, the non-conformal term $(-\frac{3b}{2}\beta_0)$ can be adopted to fix the strong running coupling. A PMC scale μ^{PMC} is then determined, which corresponds to the (correct) typical momentum flow of the process. Then, following the standard PMC procedures, the NLO decay width changes to

$$\Gamma_{\text{NLO}}^{\text{PMC}} = A \alpha_s(\mu^{\text{PMC}})^2 \left[1 + \left(a + \frac{33b}{2} \right) \alpha_s(\mu^{\text{PMC}}) \right], \quad (24)$$

where $\mu^{\text{PMC}} = \mu_R e^{3b/2}$. It is interesting to find that the PMC scale μ^{PMC} is independent to any choice of renormalization scale μ_R , e.g. $\mu^{\text{PMC}} \equiv 6.67$ GeV for B_c and $\mu^{\text{PMC}} \equiv 7.17$ GeV for B_c^* , thus the conventional renormalization scale ambiguity is really eliminated. The PMC scales are closer to $\mu_R = 2m_b$ than $\mu_R = m_w$, the conditions for the total decay widths are similar, thus the usual guessing choice of $\mu_R = 2m_b$ is more reasonable for conventional prediction. Thus in the following analysis, we fix $\mu_R = 2m_b$ for predictions when use conventional pQCD series.

	Γ_{LO} (keV)	$\Gamma_{\text{NLO,Cor.}}$ (keV)	Γ_{NLO} (keV)	$\Gamma_{\text{NLO,Cor.}}/\Gamma_{\text{LO}}$
B_c	3.53	2.05	5.58	0.58
B_c^*	2.92	0.92	3.84	0.32

TABLE III. Total decay widths of $W^+ \rightarrow B_c(B_c^*) + b + \bar{s} + X$ up to NLO accuracy under the PMC scale-setting approach.

Numerical results for the total decay widths of $W^+ \rightarrow B_c(B_c^*) + b + \bar{s} + X$ up to NLO accuracy under the PMC are shown in Table III. After applying the PMC scale-setting approach, the convergence is slightly better than conventional series, e.g. after including the NLO QCD corrections, the decay width for $W^+ \rightarrow B_c(B_c^*) + b + \bar{s} + X$ is increased by 58% (32%).

B. Comparison of the decay widths under the fixed-order and fragmentation approaches

It is interesting to know the differential distributions of those decay processes. We define the energy fraction $z \equiv E_1/E_1^{\text{max}}$, where E_1 and E_1^{max} are the energy and the maximum energy of the $B_c(B_c^*)$ meson in the rest frame of the initial W^+ boson. The differential decay widths $d\Gamma/dz$ for $W^+ \rightarrow B_c^* + b + \bar{s} + X$ are presented in Figs. 6 and 7. In addition to the fixed-order results, we also present the results from the fragmentation approach up to NLO level. Here, in order to know whether the fragmentation mechanism dominates the decay processes, we

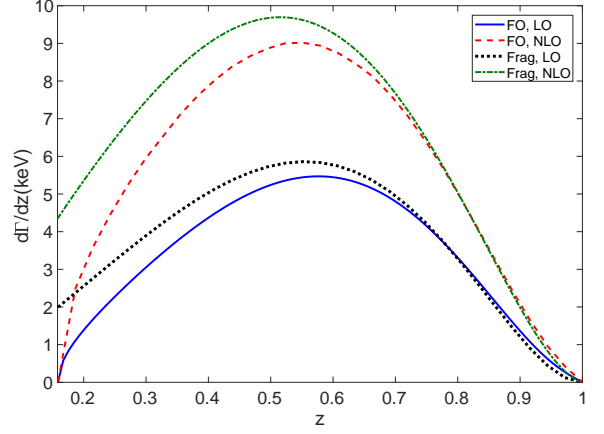


FIG. 6. The differential width $d\Gamma/dz$ for $W^+ \rightarrow B_c + b + \bar{s} + X$ under the fixed-order (FO) and fragmentation (Frag) approaches.

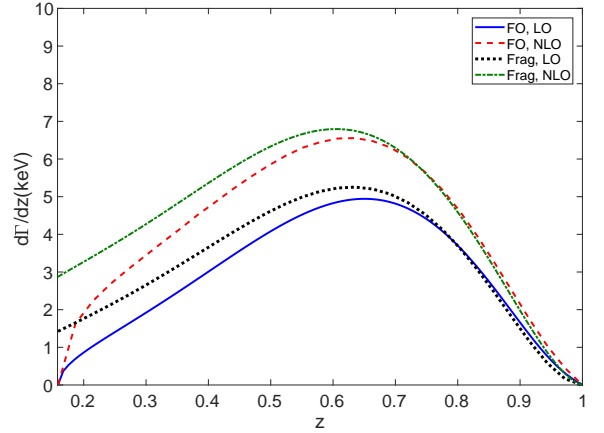


FIG. 7. The differential width $d\Gamma/dz$ for $W^+ \rightarrow B_c^* + b + \bar{s} + X$ under the fixed-order (FO) and fragmentation (Frag) approaches.

do not resum the leading logarithms of m_Q/m_w , i.e., the coefficient function and the fragmentation functions are both calculated at the LO or NLO level without the DGLAP evolution. The factorization and renormalization scales are set as $2m_b + m_c$ and $2m_b$ respectively in the fragmentation calculation.

	Frag, NLO	Frag, NLO+NLL
B_c	5.82	5.71
B_c^*	4.15	4.07

TABLE IV. The total decay widths (in unit: keV) for $W^+ \rightarrow B_c(B_c^*) + b + \bar{s} + X$ under the fragmentation approach.

Figs. 6 and 7 show that the fragmentation mechanism dominates the decay processes $W^+ \rightarrow B_c(B_c^*) + b + \bar{s} + X$, since the fixed-order and fragmentation shapes are close

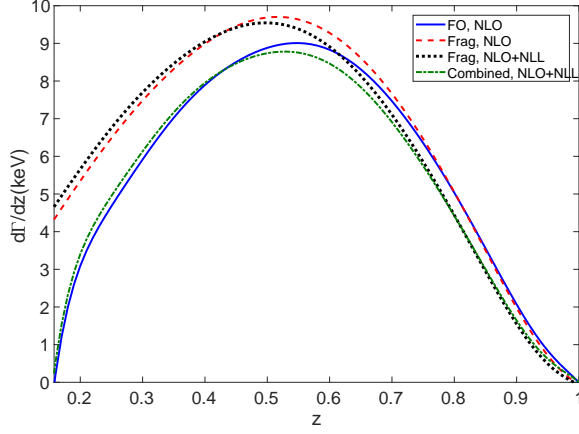


FIG. 8. The NLO differential decay width $d\Gamma/dz$ for $W^+ \rightarrow B_c + b + \bar{s} + X$ under the fixed-order approach (FO), fragmentation approach (Frag) and the combination of two approaches (Combined), respectively.

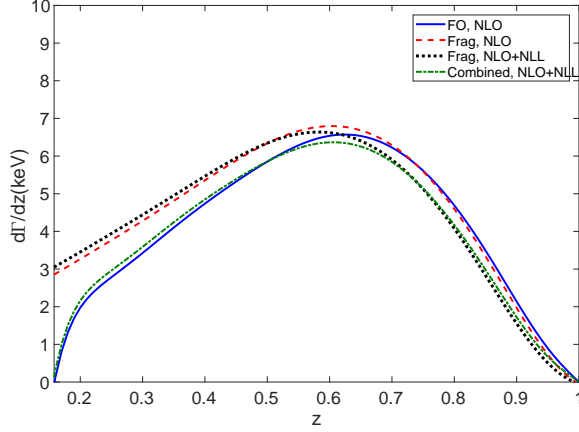


FIG. 9. The NLO differential decay width $d\Gamma/dz$ for $W^+ \rightarrow B_c^* + b + \bar{s} + X$ under the fixed-order approach (FO), fragmentation approach (Frag) and the combination of two approaches (Combined), respectively.

at the LO and NLO levels. Differences appear in small z region, indicating in this z -region, the non-fragmentation terms become important. The neglected logarithms of m_Q/m_W may give sizable contributions, which can be resummed in fragmentation approach by using the DGLAP evolution equation. More explicitly, the NLO fragmentation results without or with resummation labelled as “Frag, NLO” and “Frag, NLO+NLL” are presented in Figs. 8 and 9, which are calculated by using Eqs.(20, 21), respectively. Here the NLO fixed-order results labelled as “FO, NLO” are presented as a comparison. The decay widths for “Frag, NLO” and “Frag, NLO+NLL” are presented in Table IV. One may observe that by resumming the next-to-leading logarithms of m_Q/m_W , more accurate behavior in large z region can be achieved, and

the total decay widths shall be reduced by about 2% for both B_c and B_c^* productions.

In the fixed-order prediction, the large logarithms of m_Q/m_W may appear in specific kinematic region, and the fragmentation approach provides us a way to give a reasonable contribution in this region by resumming all the large logarithms. Thus a combination of those two approaches may be helpful. As an attempt, we combine the NLO results from the fixed-order and fragmentation approaches in the following way,

$$d\Gamma_{W^+ \rightarrow B_c^{(*)} + X}^{\text{Combined, NLO+NLL}} = d\Gamma_{W^+ \rightarrow B_c^{(*)} + X}^{\text{FO, NLO}} + \left(d\Gamma_{W^+ \rightarrow B_c^{(*)} + X}^{\text{Frag, NLO+NLL}} - d\Gamma_{W^+ \rightarrow B_c^{(*)} + X}^{\text{Frag, NLO}} \right).$$

The differential decay widths $d\Gamma/dz$ for “Combined, NLO+NLL” are also presented in Figs. 8 and 9. The total decay widths are

$$\Gamma_{W^+ \rightarrow B_c + X}^{\text{Combined, NLO+NLL}} = 4.78 \text{ keV}, \quad (25)$$

$$\Gamma_{W^+ \rightarrow B_c^* + X}^{\text{Combined, NLO+NLL}} = 3.47 \text{ keV}. \quad (26)$$

VI. SUMMARY

In the present paper, we have calculated the W^+ -boson decays, $W^+ \rightarrow B_c(B_c^*) + b + \bar{s} + X$, up to NLO QCD corrections under the NRQCD framework. Both the fixed-order and fragmentation approaches are adopted for the calculations. Our results show the NLO corrections are significant. Under conventional scale-setting approach, the decay widths for $W^+ \rightarrow B_c(B_c^*) + b + \bar{s} + X$ shall be increased by 69% (43%) for the case of $\mu_R = 2m_b$ after including the NLO corrections. The scale dependence can be suppressed after including the NLO corrections, even though it is still large. By using the PMC, we show that the renormalization scale ambiguity can be eliminated for those two decay processes; thus they provide another successful applications of the PMC.

The differential distributions $d\Gamma/dz$ for the W^+ -boson decays $W^+ \rightarrow B_c(B_c^*) + b + \bar{s} + X$ have been given under the fixed-order and the fragmentation approaches, respectively. Our results show that both decay processes are dominated by the fragmentation mechanism, and the differences exist in small z region. By combining the fixed-order prediction with the fragmentation approach to resum the leading and next-to-leading logarithms of m_Q^2/m_W^2 , a more accurate distribution to the fixed-order prediction can be achieved.

The total W -boson decay width is $\Gamma_W = 2.09 \text{ GeV}$ [65]. Using the combined results (25, 26) from the fixed-order and fragmentation approaches, we obtain the branching fractions for the considered channels, e.g.

$$\Gamma_{W^+ \rightarrow B_c + b + \bar{s} + X} / \Gamma_W = 2.29 \times 10^{-6}, \quad (27)$$

$$\Gamma_{W^+ \rightarrow B_c^* + b + \bar{s} + X} / \Gamma_W = 1.66 \times 10^{-6}. \quad (28)$$

If the LHC runs with a luminosity of $10^{34} \text{ cm}^{-2} \text{ s}^{-1}$ [36], the expected W^+ -boson events is about 3.07×10^{10} events

per operation year. Then, there are about 7.03×10^4 B_c mesons and 5.10×10^4 B_c^* mesons to be produced through the W^+ -boson decays per operation year. Two $2S$ -level excited states $B_c(2^1S_0)$ and $B_c(2^3S_1)$ have recently been observed by CMS and LHCb collaborations [66, 67]. Using $|R_{2S}(0)|^2 = 0.983 \text{ GeV}^3$ [64], there are about 4.21×10^4 $B_c(2^1S_0)$ and 3.05×10^4 $B_c^*(2^3S_1)$ to be produced through the W^+ -boson decays per operation year. Those excited states can also be important sources for the ground-state B_c meson. Thus by carefully measuring the W^+ -boson decays, we may have a good chance to

study the B_c meson properties.

Acknowledgments: This work was supported in part by the Natural Science Foundation of China under Grant No.11625520, No.11847222, No.11847301, No.11675239, No.11535002, by the Fundamental Research Funds for the Central Universities under Grant No.2019CDJDWL0005, by the China Postdoctoral Science Foundation under Grant No.2019M663432, and by the graduate research and innovation foundation of Chongqing, China under Grant No.CYB19065.

-
- [1] F. Abe, et al. (CDF Collaboration), Observation of the B_c meson in $p\bar{p}$ collisions at $\sqrt{s} = 1.8 \text{ TeV}$, Phys. Rev. Lett. **81**, 2432 (1998); Observation of B_c mesons in $p\bar{p}$ collisions at $\sqrt{s} = 1.8 \text{ TeV}$, Phys. Rev. D **58**, 112004 (1998).
 - [2] C.-H. Chang and Y.-Q. Chen, The hadronic production of the B_c meson at Tevatron, CERN LHC and SSC, Phys. Rev. D **48**, 4086 (1993).
 - [3] C.-H. Chang, Y.-Q. Chen, G.-P. Han and H.-T. Jiang, On hadronic production of the B_c meson, Phys. Letts. B **364**, 78 (1995).
 - [4] K. Kolodziej, A. Leike and R. Ruckl, Production of B_c mesons in hadronic collisions, Phys. Letts. B **355**, 337 (1995).
 - [5] A. V. Berezhnuy, A. K. Likhoded and M. V. Shevlyagin, Hadronic production of B_c mesons, Phys. Atom. Nucl. **58**, 672 (1995).
 - [6] C.-H. Chang, Y.-Q. Chen and R. J. Oakes, Comparative study of the hadronic production of B_c mesons, Phys. Rev. D **54**, 4344 (1996).
 - [7] A. V. Berezhnuy, V. V. Kiselev and A. K. Likhoded, Hadronic production of S and P wave states of anti-b c quarkonium, Z. Phys. A **356**, 79 (1996).
 - [8] S. P. Baranov, Pair production of $B_c^{(*)}$ mesons in pp and gamma gamma collisions, Phys. Rev. D **55**, 2756 (1997).
 - [9] S. P. Baranov, Semiperturbative and nonperturbative production of hadrons with two heavy flavors, Phys. Rev. D **56**, 3046 (1997).
 - [10] K. M. Cheung, B_c meson production at the Tevatron revisited, Phys. Letts. B **472**, 408 (2000).
 - [11] C.-H. Chang and X.-G. Wu, Uncertainties in estimating hadronic production of the meson B_c and comparisons between TEVATRON and LHC, Eur. Phys. J. C **38**, 267 (2004).
 - [12] C.-H. Chang, J.-X. Wang and X.-G. Wu, Hadronic production of the P-wave excited B_c -states $B_{(cJ,L=1)}^*$, Phys. Rev. D **70**, 114019 (2004).
 - [13] C.-H. Chang, C.-F. Qiao, J.-X. Wang and X.-G. Wu, The Color-octet contributions to P-wave B_c meson hadroproduction, Phys. Rev. D **71**, 074012 (2005).
 - [14] C.-H. Chang, C.-F. Qiao, J.-X. Wang and X.-G. Wu, Hadronic production of $B_c(B_c^*)$ meson induced by the heavy quarks inside the collision hadrons, Phys. Rev. D **72**, 114009 (2005).
 - [15] C.-H. Chang, C. Driouichi, P. Eerola, X.-G. Wu, BCVEGPY: An Event generator for hadronic production of the B_c meson, Comput. Phys. Commun. **159**, 192 (2004).
 - [16] C.-H. Chang, J.-X. Wang, X.-G. Wu, BCVEGPY2.0: A Upgrade version of the generator BCVEGPY with an addendum about hadroproduction of the P-wave B(c) states, Comput.Phys.Comm. **174**, 241 (2006); An Upgraded version of the generator BCVEGPY2.0 for hadronic production of B(c) meson and its excited states, Comput. Phys. Commun. **175**, 624 (2006).
 - [17] X.-Y. Wang and X.-G. Wu, A Trick to Improve the Efficiency of Generating Unweighted Events from BCVEGPY, Comput.Phys.Comm. **183**, 442 (2012).
 - [18] A.V. Berezhnuy, I.N. Belov, A.K. Likhoded and A.V. Luchinsky, B_c excitations at LHC experiments, Mod. Phys. Lett. A **34**, 1950331 (2019).
 - [19] Z. Yang, X.-G. Wu and X.-Y. Wang, BEEC: An event generator for simulating the B_c meson production at an e^+e^- collider, Comput. Phys. Commun. **184**, 2848 (2013).
 - [20] X.-C. Zheng, C.-H. Chang and Z. Pan, Production of doubly heavy-flavored hadrons at e^+e^- colliders, Phys. Rev. D **93**, 034019 (2016).
 - [21] X.-C. Zheng, C.-H. Chang, T.-F. Feng and Z. Pan, NLO QCD corrections to $B_c(B_c^*)$ production around the Z pole at an e^+e^- collider, Sci. China Phys. Mech. Astron. **61**, 031012 (2018).
 - [22] X.-C. Zheng, C.-H. Chang and T.-F. Feng, A proposal on complementary determination of the electro-weak mixing angles $\sin\theta_W$ at a super Z-factory, arXiv:1810.09393.
 - [23] X.-C. Zheng, C.-H. Chang, T.-F. Feng and X.-G. Wu, QCD NLO fragmentation functions for c or \bar{b} quark to B_c or B_c^* meson and their application, Phys. Rev. D **100**, 034004 (2019).
 - [24] H.-Y. Bi, R.-Y. Zhang, H.-Y. Han, Y. Jiang and X. G. Wu, Photoproduction of the $B_c^{(*)}$ meson at the LHeC, Phys. Rev. D **95**, 034019 (2017).
 - [25] K. He, H.-Y. Bi, R.-Y. Zhang, X.-Z. Li and W.-G. Ma, P-wave excited B_c^{**} meson photoproduction at the LHeC, J.Phys. G **45**, 055005 (2018).
 - [26] C.-F. Qiao, C.-S. Li, and K.-T. Chao, Top quark decays into heavy quark mesons, Phys. Rev. D **54**, 5606 (1996).
 - [27] C.-H. Chang, J.-X. Wang, and X.-G. Wu, Production of B_c or \bar{B}_c meson and its excited states via t-quark or \bar{t} -quark decays, Phys. Rev. D **77**, 014022 (2008).
 - [28] P. Sun, L.-P. Sun and C.-F. Qiao, Next-to-leading order corrections to top quark decays to heavy quarkonia, Phys. Rev. D **81**, 114035 (2010).
 - [29] C.-H. Chang and Y.-Q. Chen, The Production of B_c or

- \bar{B}_c associated with two heavy quark jets in Z^0 boson decay, Phys. Rev. D **46**, 3845 (1992); Erratum, Phys. Rev. D **50**, 6013 (1994).
- [30] L.-C. Deng, X.-G. Wu, Z. Yang, Z.-Y. Fang and Q.-L. Liao, Z^0 Boson Decays to $B_c^{(*)}$ Meson and Its Uncertainties, Eur. Phys. J. C **70**, 113 (2010).
 - [31] Z. Yang, X.-G. Wu, L.-C. Deng, J.-W. Zhang and G. Chen, Production of the P -Wave Excited B_c -States through the Z^0 Boson Decays, Eur. Phys. J. C **71**, 1563 (2011).
 - [32] C.-F. Qiao, L.-P. Sun and R.-L. Zhu, The NLO QCD Corrections to B_c Meson Production in Z^0 Decays, J. High Energy Phys. **08**, 131 (2011).
 - [33] J. Jiang, L.-B. Chen and C.-F. Qiao, QCD NLO corrections to inclusive B_c^* production in Z^0 decays, Phys. Rev. D **91**, 034033 (2015).
 - [34] J. Jiang and C.-F. Qiao, B_c Production in Higgs Boson Decays, Phys. Rev. D **93**, 054031 (2016).
 - [35] Q.-L. Liao and J. Jiang, Excited heavy quarkonium production in Higgs boson decays, Phys. Rev. D **100**, 053002 (2019).
 - [36] C.-F. Qiao, L.-P. Sun, D.-S. Yang and R.-L. Zhu, W boson inclusive decays to quarkonium and $B_c^{(*)}$ meson at the LHC, Eur. Phys. J. C **71**, 1766 (2011).
 - [37] Q.-L. Liao, X.-G. Wu, J. Jiang, Z. Yang and Z.-Y. Fang, Heavy quarkonium production at the LHC through W boson decays, Phys. Rev. D **85**, 014032 (2012).
 - [38] F. Feng, Y. Jia and W.-L. Sang, Optimized predictions for $W \rightarrow B_c + \gamma$ combining light-cone and NRQCD approaches, arXiv:1902.11288.
 - [39] G.T. Bodwin, E. Braaten and G.P. Lepage, Rigorous QCD analysis of inclusive annihilation and production of heavy quarkonium, Phys. Rev. D **51**, 1125 (1995) [Erratum-ibid. D **55**, 5853 (1997)].
 - [40] X.-G. Wu, S. J. Brodsky and M. Mojaza, The Renormalization Scale-Setting Problem in QCD, Prog. Part. Nucl. Phys. **72**, 44 (2013).
 - [41] X.-G. Wu, Y. Ma, S.-Q. Wang, H.-B. Fu, H.-H. Ma, S. J. Brodsky and M. Mojaza, Renormalization Group Invariance and Optimal QCD Renormalization Scale-Setting, Rep. Prog. Phys. **78**, 126201 (2015).
 - [42] X.-G. Wu, J.-M. Shen, B.-L. Du, X.-D. Huang, S.-Q. Wang and S. J. Brodsky, The QCD Renormalization Group Equation and the Elimination of Fixed-Order Scheme-and-Scale Ambiguities Using the Principle of Maximum Conformality, Prog. Part. Nucl. Phys. **108**, 103706 (2019).
 - [43] S. J. Brodsky and X.-G. Wu, Scale Setting Using the Extended Renormalization Group and the Principle of Maximum Conformality: the QCD Coupling Constant at Four Loops, Phys. Rev. D **85**, 034038 (2012).
 - [44] S. J. Brodsky and X.-G. Wu, Eliminating the Renormalization Scale Ambiguity for Top-Pair Production Using the Principle of Maximum Conformality, Phys. Rev. Lett. **109**, 042002 (2012).
 - [45] S. J. Brodsky and L. D. Giustino, Setting the Renormalization Scale in QCD: The Principle of Maximum Conformality, Phys. Rev. D **86**, 085026 (2012).
 - [46] M. Mojaza, S. J. Brodsky, and X.-G. Wu, Systematic All-Orders Method to Eliminate Renormalization-Scale and Scheme Ambiguities in Perturbative QCD, Phys. Rev. Lett. **110**, 192001 (2013).
 - [47] S. J. Brodsky, M. Mojaza, and X.-G. Wu, Systematic Scale-Setting to All Orders: The Principle of Maximum Conformality and Commensurate Scale Relations, Phys. Rev. D **89**, 014027 (2014).
 - [48] M. Beneke and V.A. Smirnov, Asymptotic expansion of Feynman integrals near threshold, Nucl. Phys. B **522**, 321 (1998).
 - [49] B.W. Harris and J.F. Owens, The Two cutoff phase space slicing method, Phys. Rev. D **65**, 094032 (2001).
 - [50] T. Hahn, Generating Feynman diagrams and amplitudes with FeynArts 3, Comput. Phys. Commun. **140**, 418 (2001).
 - [51] R. Mertig, M. Bohm and A. Denner, FeynCalc - Computer-algebraic calculation of Feynman amplitudes, Comput. Phys. Commun. **64**, 345 (1991).
 - [52] V. Shtabovenko, R. Mertig and F. Orellana, New Developments in FeynCalc 9.0, Comput. Phys. Commun. **207**, 432 (2016).
 - [53] F. Feng, \$Apart: A Generalized Mathematica Apart Function, Comput. Phys. Commun. **183**, 2158 (2012).
 - [54] A.V. Smirnov, Algorithm FIRE - Feynman Integral Reduction, J. High Energy Phys. **0810**, 107 (2008).
 - [55] T. Hahn and M. Perez-Victoria, Automatized one loop calculations in four-dimensions and D-dimensions, Comput. Phys. Commun. **118**, 153 (1999).
 - [56] G. P. Lepage, A new algorithm for adaptive multidimensional integration, J. Comp. Phys. **27**, 192 (1978).
 - [57] X.-C. Zheng, C.-H. Chang and X.-G. Wu, NLO fragmentation functions of heavy quarks into heavy quarkonia, Phys. Rev. D **100**, 014005 (2019).
 - [58] Y.L. Dokshitzer, Calculation of the Structure Functions for Deep Inelastic Scattering and e^+e^- Annihilation by Perturbation Theory in Quantum Chromodynamics, Sov. Phys. JETP **46**, 641 (1977); Zh.Eksp.Teor.Fiz. **73**, 1216 (1977).
 - [59] V.N. Gribov and L.N. Lipatov, Deep inelastic ep scattering in perturbation theory, Sov. J. Nucl. Phys. **15**, 438 (1972); Yad.Fiz. **15**, 781 (1972).
 - [60] G. Altarelli and G. Parisi, Asymptotic Freedom in Parton Language, Nucl. Phys. B **126**, 298 (1977).
 - [61] G. Curci, W. Furmanski and R. Petronzio, Evolution of Parton Densities Beyond Leading Order: The Nonsinglet Case, Nucl. Phys. B **175**, 27 (1980).
 - [62] W. Furmanski and R. Petronzio, Singlet Parton Densities Beyond Leading Order, Phys. Letts. B **97**, 437 (1980).
 - [63] E.G. Floratos, D.A. Ross and C.T. Sachrajda, Higher Order Effects in Asymptotically Free Gauge Theories. 2. Flavor Singlet Wilson Operators and Coefficient Functions, Nucl. Phys. B **152**, 493 (1979); A. Gonzalez-Arroyo and C. Lopez, Second Order Contributions to the Structure Functions in Deep Inelastic Scattering. 3. The Singlet Case, Nucl. Phys. B **166**, 429 (1980); E.G. Floratos, C. Kounnas and R. Lacaze, Higher Order QCD Effects in Inclusive Annihilation and Deep Inelastic Scattering, Nucl. Phys. B **192**, 417 (1981).
 - [64] E.J. Eichten and C. Quigg, Mesons with beauty and charm: Spectroscopy, Phys.Rev. D **49**, 5845 (1994) and references therein.
 - [65] C. Patrignani et al (Particle Data Group), Chin. Phys. C. **40**, 100001(2016).
 - [66] A.M. Sirunyan, et al.(CMS Collaboration), Observation of Two Excited B_c^+ States and Measurement of the $B_c^+(2S)$ Mass in pp Collisions at $\sqrt{s} = 13\text{TeV}$, Phys. Rev. Lett. **122**, 132001 (2019).
 - [67] R. Aaij, et al.(LHCb Collaboration), Observation of an

Excited B_c^+ State, Phys. Rev. Lett. **122**, 232001 (2019).